optica

Three-dimensional photonic crystal simultaneously integrating a nanocavity laser and waveguides: supplementary material

T. Tajiri,[1,*] S. Takahashi,[2] Y. Ota,[2] K. Watanabe,[2] S. Iwamoto,[1,2] and Y. Arakawa[1,2]

[1]Institute of Industrial Science, University of Tokyo, 4-6-1 Komaba, Meguro-ku, Tokyo 153-8505, Japan
[2]Institute of Nano Quantum Information Electronics, University of Tokyo, 4-6-1 Komaba, Meguro-ku, Tokyo 153-8505, Japan
*Corresponding author: ttajiri@iis.u-tokyo.ac.jp

This document provides supplementary information to "Three-dimensional photonic crystal simultaneously integrating a nanocavity laser and waveguides," https://doi.org/10.1364/OPTICA.6.000296. Here, we show detailed structures of the trench and plates used in the plate-insertion stacking method. The calculated field distributions of the optical modes in the integrated nanocavtiy and waveguides are also provided. Additional spatial photoluminescence images measured for the nanocavity modes in our three-dimensional (3D) photonic crystal (PC) circuit and in a reference 3D PC sample without integrated waveguides are shown and discussed.

1. Design and fabrication of trench and plate in plate-insertion stacking method

Figures S1(a)–(c) schematically show the trench and plate used for the plate-insertion stacking method. The upper part of the trench had constant width $W'_1 = 14.2$ μm and length $L'_1 = 18$ μm, as shown in the top view in Fig. S1(a), and the lower part of the trench was separated into two branches from the point where the plates were inserted and carried to the upper region for stacking. The trench pattern was formed in the top GaAs slab layer of thickness $t'_1 = 225$ nm, under which a wider space was formed in a sacrificial AlGaAs layer of thickness $t'_2 = 3$ μm, as shown in the cross-section view of the trench in Fig. S1(b). Figure S1(c) shows a top view of the plate, where the woodpile structure is formed over the area $L \times L = 11.3 \times 11.3$ μm^2. The width of the plate, defined as W in Fig. S1(c), becomes wider around the bottom part, which has height H. The shape of the plate was fitted with the trench to fulfill the relationship $W = W'_1$ and $H = t'_2$. This relationship enabled accurate stacking of the plates into the trench. The bottom edge of the plate was contoured in order to moderate Van der Waals forces between the plate and the trench during manipulation, allowing us to move plates smoothly after insertion by simply pushing the top edge with a manipulator. Three rectangular holes near the bottom edge were added to allow hydrofluoric acid to more efficiently etch the AlGaAs sacrificial layer during the wet etching process. Regarding the side edges of the plate, they were designed so that W decreased gradually from bottom to top, and near the bottom, there were air gaps of width $G = 200$ nm. The side edge design was useful for moderating friction between the plate and the trench
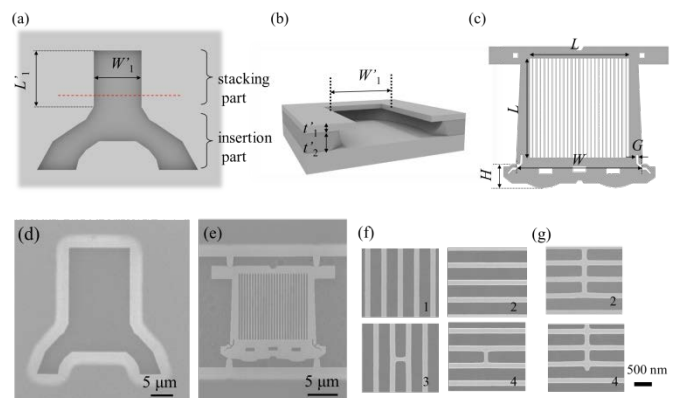

Fig. S1. (a)–(c) Design of the trench and the plate used in the plate-insertion stacking method. (a) Top view of the trench and (b) its cross-section view at the red dashed line shown in (a). (c) Top view of the plate. (d, e) Top view SEM images of a fabricated (d) plate and (e) trench. (f, g) SEM images of magnified patterns fabricated for (f) Z- and (g) Y- waveguides.

during manipulation and for avoiding fragments from intervening between the plates.

For fabrication of the trench, we used a GaAs substrate on which a 3-μm-thick AlGaAs sacrificial layer and 225-nm-thick GaAs slab layer were sequentially grown by molecular-beam epitaxy. The trench was defined by electron-beam (EB) lithography and fabricated by reactive ion etching, followed by wet etching using
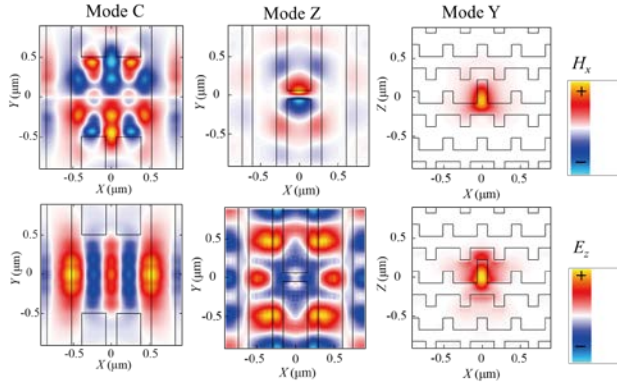
Fig. S2. Calculated cross-sectional distributions of the H_x field (upper panel) and E_z field (lower panel) for the guided nanocavity mode and the relevant Z- and Y-waveguide modes. The cross-sections are the x-y plane for the nanocavity and Z-waveguide modes and the x-z plane for the Y-waveguide mode. Black lines show the structure edge in the cut plane.

hydrofluoric acid. Since the AlGaAs layer was etched isotropically in the wet process, parts of the GaAs slab layer is suspended in air as shown in Fig. S1 (b). For fabrication of the plates, we used the fabrication procedure described in ref. [1, 2] The top view scanning electron microscopy (SEM) images of the fabricated trench and plate are shown in Fig. S1(d) and (e). The patterns for Z- and Y-waveguides are magnified in the SEM images in Fig. S1(f) and (g), respectively. These plates are stacked into the trench one-by-one using micromanipulation as shown in Fig. 3 (a) in main text under SEM observation. Although this manipulation process takes 10 minutes for stacking one plate on average, the time would be shortened by further development of manipulation technology. Regarding the areal size of the plates, it is limited currently by the fragility of the narrow rods in the patterns. The enlargement of the pattern size would be enabled by using other 3D PC designs [3, 4] thanks to their large mechanical strengths.

2. Spatial fields of optical modes relevant to 3D guiding in our 3D PC circuit

Figures S2 show the calculated cross-sectional distributions of the x-component of the magnetic field (H_x) and z-component of the electric field (E_z) for Mode C, Z and Y which are defined in Figs. 2 in the main text. The H_x distribution for the nanocavity mode (Mode C) shows the same spatial symmetry as that of the Z-waveguide mode (Mode Z). They are symmetric to the y-axis and anti-symmetric to the x-axis, allowing for coupling from the nanocavity to the Z-waveguide. The mode profiles for Mode Z and Mode Y are calculated by a plate-wave-expansion method while that for Mode C is calculated by 3D-FDTD method. The refractive index of GaAs was set as 3.4 in these calculations. Figure S3 shows the H_x field profile at y-z cross-section around the waveguide bend. It was calculated by 3D-FDTD method including all circuit components by exciting the cavity mode Mode C. Light propagating in Z-waveguide (from left in Fig. S3) is transmitted to Y-waveguide through the waveguide bend.

3. Optical measurement setup

We used a micro-photoluminescence (PL) measurement setup for optical characterization of our 3D PC circuit. In this setup, laser
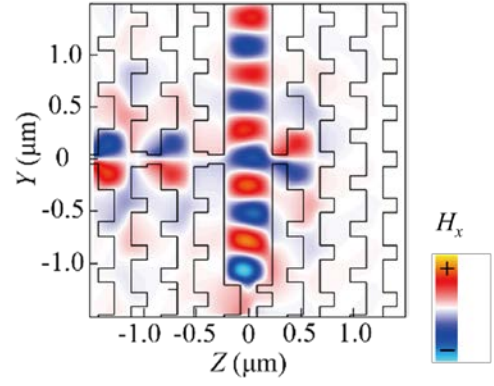

Fig. S3. Calculated y-z cross-sectional distributions of the H_x field at the waveguide bend where Z- and Y- waveguides are connected. Black lines show the structure edge in the cut plane.

pulses with a width of 8 ns at a wavelength of 905 nm were focused on the nanocavity in order to pump quantum dots (QDs)from the top of the sample with a 50× objective lens of NA = 0.65 at a repetition rate of 25 kHz. The PL signals were collected by the same objective lens and were detected using a spectrometer equipped with a 2D InGaAs detector array for measuring the spatial and spectral distributions of the PL intensity. Spatial resolution (pixel size) for measured PL images was estimated as 380 nm by 380 nm with a PL image measured for another sample with QDs embedded in two distant stacked plates.

4. Spatial PL images for 3D PC without integrated photonic waveguides

Figure S4 shows spatial PL images measured from a 3D PC that integrates only the nanocavity and does not include waveguides. A spectral peak at 1104-nm wavelength is extracted using the band pass filter (BPF) of 10-nm bandwidth. No optical spot was observed near the position (x, z) = (0, 5.3 μm) for z-polarization in Fig. S4 (a), in contrast to the PL image measured from the 3D PC with waveguides shown in Fig. 4(d) in the main text, which also indicates that the bright spot observed in Fig. 4(d) in the main text surely radiated from the output port. Regarding x-polarization, high intensity was observed around the position (x, z) = (0, 3.4 μm). This intensity could be caused by scattering due to the displaced plates in this sample.
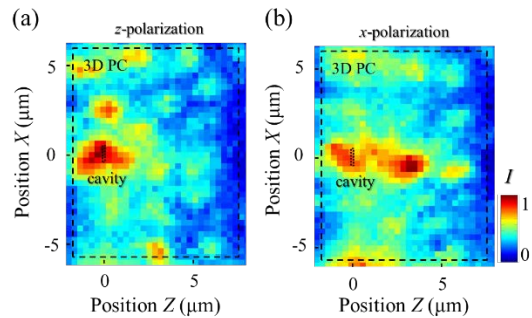

Fig. S4. Spatial PL images measured from 3D PCs without waveguides for (a) z- and (b) x- polarization. Color bar is normalized by the same value in (a) and (b). The dimensions of the 3D PC and the point defect nanocavity are shown by dashed lines.
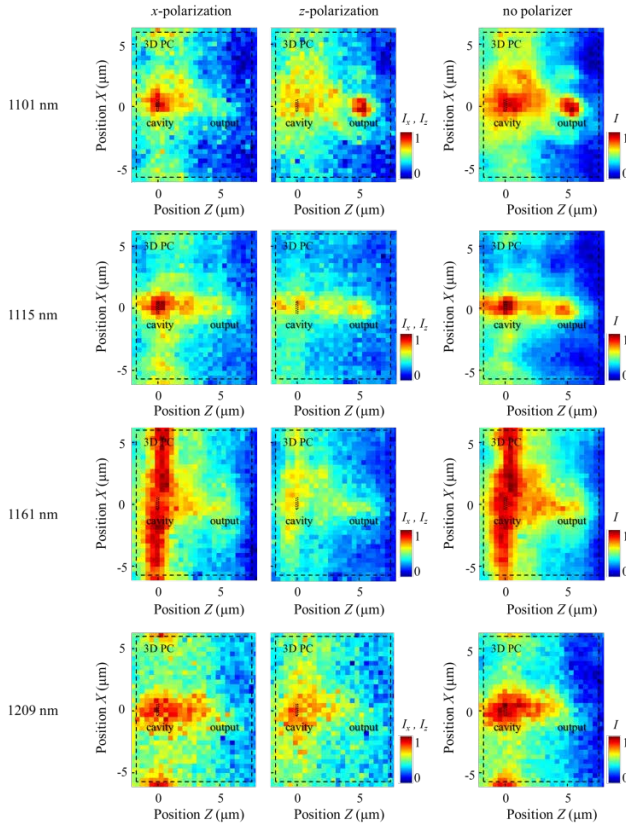
Fig. S5. Polarization dependence of the spatial PL images for spectral peaks at different wavelengths. The wavelengths of the peaks are shown in the left column. The x- and z-polarized images are shown in the left and center column, respectively, while the image measured without polarizer is shown in the right column. Color scales of the polarized images are normalized by the same value for each wavelength. The dimensions of the 3D PC and the point defect nanocavity are shown by dashed lines.

Fig. S6. (a) Measured PL spectra for z- and x- polarization components of the nanocavity mode. (b) Measured spatial PL image for the x-polarization component of the nanocavity mode. (c) Calculated spatial distribution of the +y-component of energy flux for the x-polarized component of a guided nanocavity mode. The color scale range in (b) and (c) is normalized by the same value as that in Fig. 4(d) and (e) in the main text, respectively The dimensions of the 3D PC and the point defect nanocavity are shown by dashed lines in (b) and (c).

5 Spatial PL images for spectral peaks observed from the 3D PC circuit

Figure S5 shows measured spatial PL images for nanocavity modes extracted using a BPF of 10-nm bandwidth at wavelengths left and center columns, respectively, show the x- and z- polarized components, which were extracted by a polarizer. The images of 1101 nm, 1115 nm, 1161 nm, and 1209 nm. At those wavelengths, spectral peaks were observed, as shown in the PL spectrum in Fig. 4(a) in the main text. In Fig. S5, the images at the measured with no polarizer are shown for reference in the right column. In addition to the bright spot near the output port position $(x, z) = (0, 5.3~\mu m)$ for z-polarization at 1101-nm wavelength, a weak optical spot was also observed near the same position for z-polarization at 1115-nm wavelength. This weak optical spot could also be considered to be light guided from the nanocavity via the waveguide, although its guiding efficiency would be low for this nanocavity mode as suggested by the weak intensity. In the 3D finite-difference time-domain (FDTD) calculation including all photonic circuit components, there were two nanocavity modes that were guided through the waveguides from the nanocavity at the wavelengths of
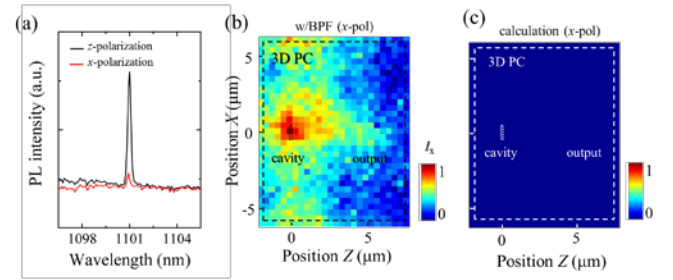
1207 nm and 1179 nm. Although the wavelengths of the guided nanocavity modes were blue-shifted by about 100 nm in experiment, such blue-shift could be caused by fabrication imperfections such as narrowed widths of rods in the woodpile structure. Regarding the other spectral peaks observed at 1161 nm and 1209 nm in experiment, the spatial PL images in Fig. S5 do not show clear optical spots near the output port position. These peaks could be considered as nanocavity modes uncoupled with the waveguides and radiated directly from the nanocavity.

6. Polarization dependence of the guided nanocavity mode measured from the 3D PC circuit

Figure S6(a) shows the PL spectra of the guided nanocavity mode for the x- and z-polarization with red and black curves, respectively. The x-polarized light was observed to have a much lower intensity than the z-polarized light. In the spatial PL image for x-polarization in Fig. S6(b), the optical spot was not observed around the output port position, in contrast to the bright optical spot observed for z-polarization at the output port position in Fig. 4 (d) in the main text. This result indicates that the output light from this waveguide is highly z-polarized. This observation was also confirmed by calculation using the 3D-FDTD method. The guided nanocavity mode showed no clear output for the x-polarization component, as shown in Fig. S6(c) at the waveguide port.

1. A. Tandechanurat, S. Ishida, D. Guimard, M. Nomura, S. Iwamoto and Y. Arakawa, Nature Photon. **5**, 91 (2011).
2. K. Aoki, D. Guimard, M. Nishioka, M. Nomura, S. Iwamoto and Y. Arakawa, Nat. Photon. **2**, 688 (2008).
3. L. Lu, L. L. Cheong, H. I. Smith, S. G. Johnson, J. D. Joannopoulos, and M. Soljačić, Opt. Lett. **37**, 4726 (2012).
4. K. Aoki, Appl. Phys. Lett. **95**, 191910 (2009).